

# Towards Distinct Element Method Simulations of Carbon Nanotube Systems

**Tyler Anderson**

Department of Mechanical Engineering  
University of Minnesota  
Minneapolis, Minnesota 55455

**Evgeniya Akatyeva**

Department of Mechanical Engineering  
University of Minnesota  
Minneapolis, Minnesota 55455

**Ilia Nikiforov**

Department of Mechanical Engineering  
University of Minnesota  
Minneapolis, Minnesota 55455

**David Potyondy**

Itasca Consulting Group, Inc.  
111 Third Avenue South,  
Minneapolis, Minnesota 55401

**Roberto Ballarini**

Department of Civil Engineering  
University of Minnesota  
Minneapolis, Minnesota 55455

**Traian Dumitrică\***

Department of Mechanical Engineering  
University of Minnesota  
Minneapolis, Minnesota 55455  
Email: td@me.umn.edu

*We propose distinct element method modeling of carbon nanotube systems. The atomic-level description of an individual nanotube is coarse-grained into a chain of spherical elements that interact by parallel bonds located at their contacts. The spherical elements lump multiple translational unit cells of the CNT, and have both translational and rotational degrees of freedom. The discrete long ranged interaction between nanotubes is included in a van der Waals contact model of non-mechanical nature that acts simultaneously with the parallel bonds. The utility of the model is demonstrated by simulating carbon nanotube rings.*

## Nomenclature

- $r$  The nanotube radius.  
 $Y, G$  Young and shear moduli of a carbon nanotube.  
 $m, R$  Mass and radius of a distinct spherical element.  
 $T, r$  The length and radius of the parallel bond.  
 $k_n, k_s$  Normal and shear stiffness of a parallel bond.  
 $\epsilon', A, \text{ and } B$  Parameters for the van der Waals contact model.  
 $L$  Intertube center-to-center distance.  
 $D$  Normalized intertube center-to-center distance  $D = (L/r) - 2$ .

## 1 Introduction

Carbon nanotubes (CNTs) exhibit remarkable mechanical characteristics, such as high mechanical strength [1] and resilience [2]. For this reason, they are highly researched for applications. Valuable insights into individual CNT response have been obtained theoretically from atomic-level simulations [1–5]. Unfortunately, performing exhaustive simulations at atomistic scale for CNT systems of engineering significance is computationally prohibitive. Coarse-graining approaches, that reduce [6,7] or even eliminate [8,9] the large number of atomistic degrees of freedom, are used in order to make simulations manageable. However, in spite of such developments, simulations on collective behavior have not kept pace with the demand from many areas, ranging from nanoelectromechanical systems [10], nanocomposite materials [11], nanotoxicology [12] and rock mechanics [13].

To model large scale motions of polymers, colloids, surfactants, nanotubes, and bio-molecular assemblies, mesoscopic simulation methods have been developed, such as dissipative particle dynamics [14] and Langevin dynamics [15]. Interestingly, the method invoked here, the distinct element method (DEM) [16], is currently used for larger scale simulations in granular and discontinuous materials, such as granular flows, powder mechanics, and rock mechanics. In this work we show that DEM can be easily adapted for CNT simulations. We first formulate a basic DEM mesoscopic model of CNT systems in terms of the contact interactions between

---

\*Address all correspondence to this author.

the discrete elements. Using parameters derived previously from the atomic-level description, we illustrate the utility of this model in a complex situation involving large elastic deformation and van der Waals (vdW) adhesion. DEM emerges as an attractive methodology not only because of its simplicity, but also because of its availability in several commercially available distinct-element programs, such as PFC3D [17] (which was used to perform the work described here). It may also be possible to perform similar modeling with traditional molecular dynamics programs, such as LAMMPS [18].

## 2 Distinct element method for CNTs

Unlike other particle-based method, the DEM particles are no longer being treated as point masses. Instead, each individual element is a rigid body characterized by a mass  $m$  uniformly distributed in the spherical element of radius  $R$  and moment of inertia  $I = (2/5)mR^2$ . These parameters are time-independent and, for simplicity, here all spheres are taken to be identical. Thus, the system composed of a collection of  $N$  discrete element contains not only translational but also rotational degrees of freedom. Specifically, the generalized coordinates (also called state variables) are the positions  $\mathbf{r}_i$  and velocities  $\mathbf{v}_i$  for the center of mass of each sphere, as well as their angular rotations  $\Theta_i$  and angular velocities  $\Omega_i$  vectors, where  $i = 1, \dots, N$ .

One counterintuitive aspect is that although the spherical particles are rigid, they can interpenetrate, Fig. 1. The intersection of the two proximate spherical surfaces define a plane, the contact plane, perpendicular to the axis connecting the two centers located at  $\mathbf{r}_i$  and  $\mathbf{r}_{i+1}$ . In the DEM logic, interpenetration signifies that the two elements interact. Various constitutive contact models of pure mechanical nature are available [17] to describe the interaction of elements. The mechanical behavior of this system is described by evolving in time each rigid sphere according to the laws of classical mechanics,  $\mathbf{F}_i = m\ddot{\mathbf{r}}_i$  and  $\mathbf{M}_i = I\ddot{\Theta}_i$ .  $\mathbf{F}_i$  and  $\mathbf{M}_i$  are the total force and moment, respectively, acting on element  $i$ , that arise due to the interactions with the elements in contact as well as artificially introduced dissipative forces. With the PFC3D method at hand [17], the system is evolved in time with a non-symplectic leapfrog second-order in time-step scheme. The goal is to drive the system towards a low energy metastable state rather than performing thermodynamic integration like in molecular dynamics.

### 2.1 Contact model to represent the covalent binding

The individual CNT quasi-one dimensional structure extending over microns of length originates in the strong covalent carbon-carbon bonding. This bonding is formed by sharing of the valence electrons, according to the laws of quantum mechanics. Paramount to our coarse-grained DEM model is describing the larger scale mechanics. Thus, we aim to retain from the fundamental atomic scale both the quasi-one dimensional stable structure and the low-frequency acoustic vibrations.

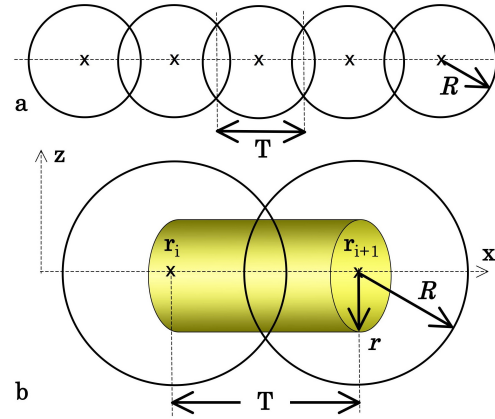


Fig. 1. (color online) (a) CNT representation as a chain of overlapping spherical elements, shown here in 2D. (b) Parallel bond contact model for the interaction of two spherical elements with radius  $R$ .

As reviewed on a number of occasions [19], the nanomechanics of deformed CNTs can be interpreted with the heuristics of the continuum. For example, a quadratic variation of strain energy with the applied strain computed microscopically is usually interpreted as linear elastic behavior. Recent microscopic data indicated that single-walled CNTs of moderate diameters can be well represented as isotropic elastic continuum shells, as earlier proposed [2]. Under large tensile stress, CNTs fail irreversibly through plasticity or brittle fracture [1]. However, microscopic calculations indicated that CNT also exhibit a rich nonlinearly elastic behavior over wide ranges of mechanical stress [2, 4, 5]. With the DEM approximation, the continuum behavior can be well reproduced. Thus, the known atomic-scale nanomechanical behavior suggests that the existing DEM clumping structure valid for the macro-scale can be used and there is no need to invent a new contact model for this purpose.

The high degree of crystalline uniformity of CNTs naturally associates one spherical element with one translational cell or supercell repeating unit with length  $T$  and containing  $N_a$  atoms. Thus, in the stress-free representation of a CNT, the distance between contact planes is  $T$ , Fig. 1(a). It is important to recognize that to comply with the underlying atomic-scale description, the translational fragments lumped into the discrete elements cannot be kept frozen during the relative motion of proximate elements with respect to each other. From the existing contact models we found adequate the standard parallel-bond contact because it establishes an elastic interaction between particles in terms of both forces and moments. (The nomenclature used highlights that this contact can work in parallel with other contact models.)

A parallel bond can be envisioned as a finite-sized disk of elastic massless material with radius  $r$  bound around the contact and centered on the axis connecting the centers of two proximate elements, Fig. 1(b). To this disk we associate a set of ideal elastic springs with normal  $k_n$  and shear  $k_s$  stiffnesses uniformly distributed over its circular cross-section. When the contact is formed in DEM, the total contact force and moment are initialized to zero. A mechanical deforma-

tion will reflect in displacements of the generalized coordinates with respect with their initial position, and contact elastic forces and moments acting to restore the needlelike shape. The restoring force and a moment develop within the bond material according to its constitutive law. For example, a  $\delta x$  axial relative displacement between  $i$  and  $i + 1$  elements causes a contact restoring force  $F_i^x = -F_{i+1}^x = -k_n S \delta x$ , while a  $\delta \Theta^z$  relative angular displacement causes a contact restoring moment  $M_i^x = -M_{i+1}^x = -k_s I_x \delta \Theta^z$ . Here  $S = \pi r^2$  and  $I_x = (\pi/2)r^4$  are the area and the polar moment of inertia of the disk cross-section. The full description of the parallel-bond implementation in PFC3D can be found in Potyondy and Cundall [13].

The two spring constants can be obtained by considering elastic elongation and torsion deformations and equating the strain energy of the DEM model with the one obtained microscopically. It follows that the length of the parallel bond disk is  $T$  and,  $k_n = Y/T$  and  $k_s = G/T$ . Here  $Y$  and  $G$  are atomistically-computed Young's and shear moduli, respectively.

## 2.2 Contact model to represent the vdW interactions

To be able to simulate CNT systems, the parallel bonds representing the covalent binding must be supplemented with a new contact force representing the vdW interaction between the two underlying parallel nanotube segments of length  $T$ . Fortunately this interaction can be captured in a simple analytical form. As usually, the vdW interaction between two atoms located at distance  $d$  is represented by a Lennard-Jones (LJ) 6-12 potential,  $v(d) = 4\epsilon \left[ (\sigma/d)^{12} - (\sigma/d)^6 \right]$ , where  $\epsilon$  and  $\sigma$  are standard parameters<sup>1</sup>. We treat the discrete interaction between carbon atoms located on the two parallel tube segments of length  $T$  in continuum way, in terms of area density of atoms  $\rho_c = 4/(3\sqrt{3}a_{C-C}^2)$  [20]. Here  $a_{C-C} = 1.42 \text{ \AA}$  is the equilibrium carbon-carbon bond length in graphene. Integrating the LJ interaction over the surfaces of the two tube segments located at a center to center distance  $L$ , we arrived at (see Appendix)

$$V(D) \approx 4\epsilon' \left[ \frac{A}{D^{9.5}} - \frac{B}{D^{3.5}} \right]. \quad (1)$$

Here  $D = (L/r) - 2$  is the normalized intertube center-to-center distance and  $\epsilon' = (\frac{3\pi\sigma^6}{8r^3} \rho_c^2 T) \epsilon$ .  $A = \frac{21\sigma^6}{32r^6} a$ , and values of dimensionless constants  $a$  and  $B$  are given in the Appendix. This simple form for the vdW interaction energy  $V$  makes it easy to derive the vdW force component acting on the spherical elements. While this model assumes that each DEM ball only interacts with its nearest neighbor in the adjacent nanotube segment, it may be easily adapted to the case of multiple-neighbor interactions, such as when the DEM balls are finely spaced.

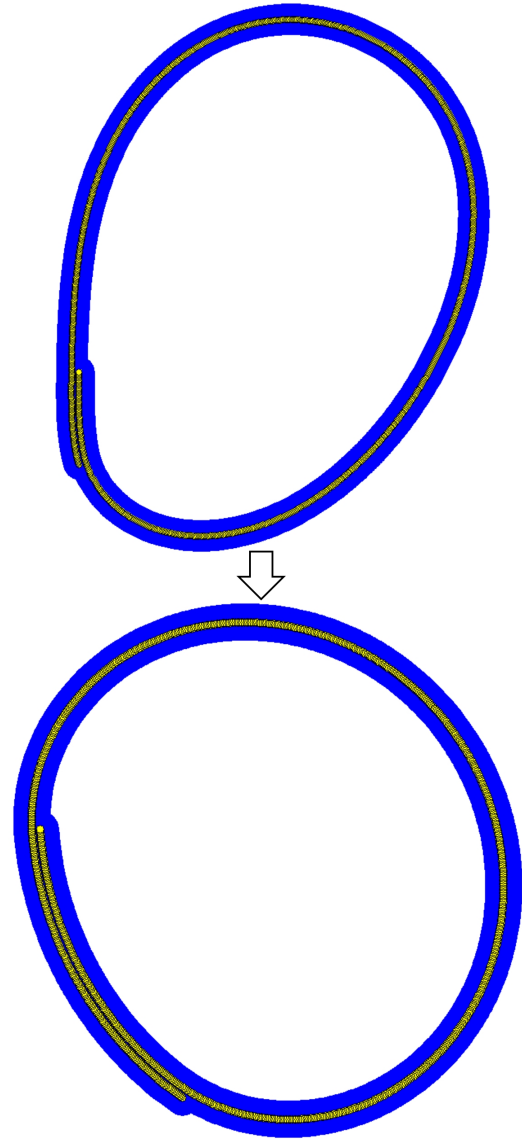


Fig. 2. (color online) Result of (5,5)@(10,10)@(15,15) MWCNT ring simulation, showing initial and final configuration of relaxation. Yellow (light gray) represents the size of the CNT, while blue (gray) represents the vdW cutoff radii of each ball.

## 3 Model parameterization and Simulations

We now show an example of how the DEM framework may be applied to CNTs. The DEM parametrization of a (5,5)@...@(15,15) multi-walled (MW) CNT is given in Tables 1, 2, and 3. This MWCNT was parametrized as an elastic cylinder for use in the PFC3D simulations. This is a natural choice given the fact that the parallel bonds represent elastic cylinders. The approximation does not introduce significant inaccuracies, especially when the primary mode of deformation is bending, as the space inside the (5,5) that is empty in the real CNT contributes less than 2% to its moment of inertia. The empty space contributes less than 12% to the cross-sectional area of the cylinder. Parallel bond radius  $r$  is set to the radius of the outer (15,15) wall,  $10.17 \text{ \AA}$ . Each

<sup>1</sup>Here we used  $\sigma = 3.851 \text{ \AA}$  and  $\epsilon = 4.0 \text{ meV}$

DEM sphere lumps two translational unit cells of the armchair MWCNT, so the element spacing  $T$  is 5.06 Å. Each sphere then lumps 240 carbon atoms, giving each sphere a mass  $m = 2,880$  amu, important if the dynamics are to be studied. The bending stiffness  $EI_x$  of this MWCNT, 12.0 eV- $\mu\text{m}$ , taken from a previous atomistic study [5] was used to calculate the Young's modulus of the elastic cylinder representing the MWCNT,  $E = 2.29$  TPa. The elastic modulus in shear was taken as the surface shear modulus of graphene multiplied by the inter-wall spacing of the MWCNT, 3.4 Å. The result is  $G = 459$  GPa. It was shown that only the innermost tubes' moduli are likely to slightly deviate from this value [3]. The error caused is further reduced by the fact that the fictitious area occupied by the inner walls contributes a comparatively small portion to the area and polar moment of the cylinder. Appropriately scaling by  $T$ , the discrete normal and shear stiffnesses for each parallel bond are then  $k_n = 2.81$  eV/Å<sup>4</sup> and  $k_s = 0.57$  eV/Å<sup>4</sup>. Because the discrete elements must interpenetrate to interact, the radius of the discrete elements,  $R = 25.4$ , is one-half the cutoff radius for the vdW interaction.

Table 1. DEM parameterization for a (5,5)@...@(15,15) MWCNT.

$m$ (amu)	$R$ (Å)
2,880	25.4

Table 2. Parallel bond parameterization for a (5,5)@...@(15,15) MWCNT.

$T$ (Å)	$r$ (Å)	$k_n$ (eV/Å <sup>4</sup> )	$k_s$ (eV/Å <sup>4</sup> )
5.06	10.17	2.81	0.57

Table 3. Van der Waals bond parameterization for the interaction of (5,5)@...@(15,15) MWCNTs.

$\epsilon'$ (meV)	$A$	$B$
10.77	$9.15 \cdot 10^{-4}$	1.31

Having the model parameterized, we now demonstrate its utility in describing the MWCNT rings often encountered in experiment [21]. This represents an ideal test for

the model since the ring structure arises from the energy balance stored in the parallel and vdW bonds. Simulations considered a (5,5)@(10,10)@(15,15) MWCNT of 500nm length contains 240,000 atoms, a system well beyond the comfortable computational level of atomistic or FEM simulations. This MWCNT is represented by 1,000 DEM balls.

Starting from a strait configuration, the tube was gradually bended accumulating strain in the parallel bonds. The remarkable part of the simulations starts from the moment when the two ends were brought into the range of the vdW interaction. Fig. 2 shows the result of this last part, which lasted about two hours on a common laptop computer. The configuration evolved from the initial state shown on the top obtained by direct bending to the final stable state on the bottom resulted by sliding in the overlap region, as well as elastic relaxation. The final ring configuration represents a minimum-energy state in the balance between vdW and elastic energy. The curvature of the ring is less than 0.2 nm<sup>-1</sup>, placing it well within the linear elastic regime of bending [5].

## 4 Conclusion

On the surface, it could be difficult to see what a methodology designed for large-scale engineering problems has to do with CNT systems. In this paper we indicated the suitability of this methodology on a much smaller time- and size-scale. We represented each CNT with a chain of parallel-bonded spherical elements to capture the intra-wall interactions along with a vdW model to capture inter-wall interactions. The resulting mesoscale model is adequate for implementation in existing DEM software packages. With the PFC3D code, we demonstrates its ability to describe CNT rings. Of course, the basic CNT mesoscopic model introduced here can be further optimized and enhanced. For example, the parallel bonds can be adjusted to accommodate nonlinear rippling by introducing a reduction in the relevant elastic constants beyond certain strain levels [5]. To describe CNT fracture, one can introduced bond strengths beyond which the parallel bonds break [1]. There is an interesting prospect for more complex engineering investigations since the foundations are already in place. For example, this method can be used to describe CNT agglomerates, of high importance to nanotoxicology.

## Acknowledgements

We thank NSF CAREER Grant No. CMMI-0747684 and Itasca Education Partnership program.

## Appendix

Equation (1) is an approximate evaluation of the vdW interaction energy given by the integral:

$$V(D) = \rho_c^2 r^2 T \int_{-\pi}^{\pi} \int_{-\pi}^{\pi} \int_{-T/2}^{T/2} v(d) dx d\theta_2 d\theta_1. \quad (2)$$

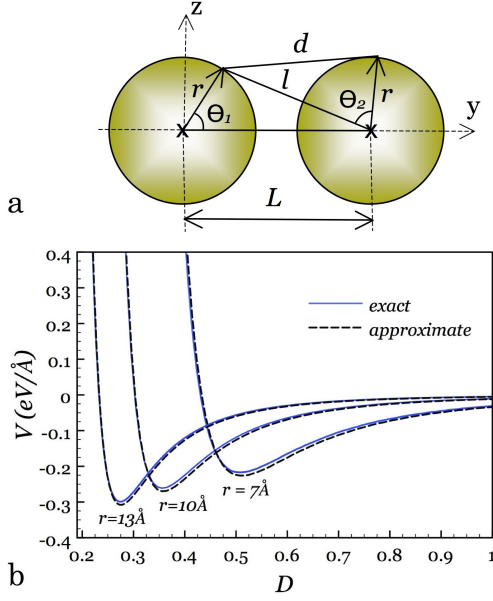


Fig. 3. (color online) (a) Schematics for the cross sectional view of two parallel tubes. (b) The vdW energy vs. a normalized intertube center-to-center distance  $D$ . Results are shown for three different tube radii. Both the exact Eqn. (2) (numerical integration) and the approximate Eqn. (1) evaluations are presented for a comparison.

In cylindrical coordinates  $(r, \theta, x)$ , the distance between two atoms located on two different tube segments aligned along the  $x$  axis is  $d = \sqrt{r^2 + l^2 - 2rl \cos \theta_2 + x^2}$ , where  $l = \sqrt{r^2 + L^2 - 2rL \cos \theta_1}$ , Fig. 3(a). We are focusing on the case in which the distance between tubes is small, which means  $D \ll 1$ . Then, the major contribution to Eqn. (2) comes from small angles  $\theta_1$  and  $\theta_2$ . It is convenient to introduce the notation  $t = \sqrt{r^2 + l^2 - 2rl \cos \theta_2}$ . Then,  $t/r \ll 1$ . If  $T \sim r$ , also  $t/T \ll 1$ . Using these approximations in the attraction and repulsive terms of Eqn. (2), it follows

$$\int_{-T/2}^{T/2} \frac{dx}{d^6} = \int_{-T/2}^{T/2} \frac{dx}{(t^2 + x^2)^3} = \frac{3\pi}{8} \frac{1}{t^5} \left[ 1 + O\left(\frac{t}{T}\right) \right],$$

$$\int_{-T/2}^{T/2} \frac{dx}{d^{12}} = \int_{-T/2}^{T/2} \frac{dx}{(t^2 + x^2)^6} = \frac{63\pi}{256} \frac{1}{t^{11}} \left[ 1 + O\left(\frac{t}{T}\right) \right].$$

Neglecting the higher order terms, Eqn. (2) writes

$$V(D) \approx \epsilon \rho_c^2 T \frac{3\pi\sigma^6}{2r^3} \int_{-\pi}^{\pi} \int_{-\pi}^{\pi} \left[ \frac{21\sigma^6}{32r^6} \left(\frac{r}{t}\right)^{11} - \left(\frac{r}{t}\right)^5 \right] d\theta_2 d\theta_1. \quad (3)$$

Further, using a Taylor series expansion

$$\frac{t^2}{r^2} = \theta_2^2 + (D + \theta_1^2)^2 + o(\max\{\theta_2^2, \theta_1^4, D\theta_1^2, D^2\}), \quad (4)$$

and substituting Eqn. (4) into Eqn. (3), one recovers Eqn. (1). The constants  $a$  and  $B$  are given by

$$a = \int_{-\infty}^{\infty} \int_{-\infty}^{\infty} \frac{dt_1 dt_2}{(t_2^2 + (1+t_1^2)^2)^{11/2}} \approx 0.47,$$

$$B = \int_{-\infty}^{\infty} \int_{-\infty}^{\infty} \frac{dt_1 dt_2}{(t_2^2 + (1+t_1^2)^2)^{5/2}} \approx 1.31.$$

The comparison for the vdW energy Eqn. (2) obtained by numerical integration against the approximate form given by Eqn. (1) is presented in Fig. 3(b) for three values of  $r$ . The small-intertube approximation behind Eqn. (1) works very well, even for large  $D$  values. This is because the exact interaction energy at large distances is negligibly small.

## References

- [1] Dumitrică, T., Hua, M., and Yakobson, B., 2006. “Symmetry-, time-, and temperature-dependent strength of carbon nanotubes”. *Proc. Natl. Acad. Sci. U.S.A.*, **103**(16), pp. 6105–6109.
- [2] Yakobson, B., Brabec, C., and Bernholc, J., 1996. “Nanomechanics of carbon tubes: Instabilities beyond linear response”. *Phys. Rev. Lett.*, **76**(14), pp. 2511–2514.
- [3] Zhang, D.-B., and Dumitrică, T., 2008. “Elasticity of ideal single-walled carbon nanotubes via symmetry-adapted tight-binding objective modeling”. *Appl. Phys. Lett.*, **93**, pp. 031919–031921.
- [4] Zhang, D.-B., James, R., and Dumitrică, T., 2009. “Electromechanical characterization of carbon nanotubes in torsion via symmetry adapted tight-binding objective molecular dynamics”. *Phys. Rev. B*, **80**(11), pp. 115418–115422.
- [5] Nikiforov, I., Zhang, D.-B., James, R., and Dumitrică, T., 2010. “Wavelike rippling in multiwalled carbon nanotubes under pure bending”. *Appl. Phys. Lett.*, **96**, pp. 123107–123109.
- [6] Buehler, M., Kong, Y., and Gao, H., 2004. “Deformation mechanisms of very long single-wall carbon nanotubes subject to compressive loading”. *Eng. Mater. Technol.*, **126**(3), pp. 245–249.
- [7] Zhigilei, L., Wei, C., and Srivastava, D., 2005. “Mesoscopic model for dynamic simulations of carbon nanotubes”. *Phys. Rev. B*, **71**(16), pp. 165417–165428.
- [8] Arroyo, M., and Belytschko, T., 2003. “Nonlinear mechanical response and rippling of thick multiwalled carbon nanotubes”. *Phys. Rev. Lett.*, **91**(21), pp. 215505–215508.
- [9] Pantano, A., Boyce, M., and Parks, D., 2003. “Nonlinear structural mechanics based modeling of carbon nanotube deformation”. *Phys. Rev. Lett.*, **91**(14), pp. 145504–145507.
- [10] Tomblar, T., Zhou, C., Alexseyev, L., Kong, J., Dai, H., Liu, L., Jayanthi, C., Tang, M., and Wu, S., 2000. “Reversible electromechanical characteristics of car-

bon nanotubes under local-probe manipulation”. *Nature London*, **405**, pp. 769–772.

- [11] Vaia, R., and Krishnamoorti, R., eds., 2001. *Polymer nanocomposites: processing, characterization, and applications*. American Chemical Society, Washington, DC.
- [12] Poland, C., Duffin, R., Kinloch, I., Maynard, A., Wallace, A. H., Seaton, A., Stone, V., Brown, S., MacNee, W., and Donaldson, K., 2008. “Carbon nanotubes introduced into the abdominal cavity of mice show asbestos-like pathogenicity in a pilot study”. *Nature Nanotech.*, **3**, pp. 423–428.
- [13] Potyondy, D., and Cundall, P., 2004. “A bonded-particle model for rock”. *Int. J. Rock Mech. & Min. Sci.*, **41**(8), pp. 1329–1364.
- [14] Hoogerbrugge, P., and Koelman, J., 1992. “Simulation microscopic hydrodynamic phenomena with dissipative particle dynamics”. *Europhys. Lett.*, **19**(3), pp. 155–160.
- [15] Smith, D., and Harris, C., 1990. “Generalized brownian dynamics. i. numerical integration of the generalized langevin equation through autoregressive modeling of the memory function”. *J. Chem. Phys.*, **92**(2), pp. 1304–1311.
- [16] Cundall, P., and Strack, O., 1979. “A discrete numerical model for granular assemblies”. *Geotechnique*, **29**(1), pp. 47–65.
- [17] Itasca Consulting Group Inc., 2008. *PFC3D (Particle Flow Code in 3 Dimensions), Version 4.0*. Minneapolis: ICG.
- [18] Plimpton, S., 1995. “Fast parallel algorithms for short-range molecular dynamics”. *J. Comput. Phys.*, **117**(1), pp. 1–19.
- [19] Dumitrică, T., ed. 2010. *Trends in Computational Nanomechanics: Transcending Length and Time Scales*. Springer.
- [20] Girifalco, L., Hodak, M., and Lee, R., 2000. “Carbon nanotubes, buckyballs, ropes, and a universal graphitic potential”. *Phys. Rev. B*, **62**(19), pp. 13104–13110.
- [21] Martel, R., Shea, H., and Avouris, P., 1999. “Rings of single-walled carbon nanotubes”. *Nature*, **398**, p. 299.